

8-1-2002

## On Using the Equivalent Conductivity to Characterize Solute Spreading in Environments with Low-Permeability Lenses

Andrew J. Guswa  
*Smith College, aguswa@smith.edu*

David L. Freyberg  
*Stanford University*

Follow this and additional works at: [https://scholarworks.smith.edu/egr\\_facpubs](https://scholarworks.smith.edu/egr_facpubs)



Part of the [Engineering Commons](#)

---

### Recommended Citation

Guswa, Andrew J. and Freyberg, David L., "On Using the Equivalent Conductivity to Characterize Solute Spreading in Environments with Low-Permeability Lenses" (2002). Engineering: Faculty Publications, Smith College, Northampton, MA.  
[https://scholarworks.smith.edu/egr\\_facpubs/38](https://scholarworks.smith.edu/egr_facpubs/38)

This Article has been accepted for inclusion in Engineering: Faculty Publications by an authorized administrator of Smith ScholarWorks. For more information, please contact [scholarworks@smith.edu](mailto:scholarworks@smith.edu)

# On using the equivalent conductivity to characterize solute spreading in environments with low-permeability lenses

Andrew J. Guswa

Picker Engineering Program, Smith College, Northampton, Massachusetts, USA

David L. Freyberg

Department of Civil and Environmental Engineering, Stanford University, Stanford, California, USA

Received 20 March 2001; revised 28 February 2002; accepted 4 March 2002; published 3 August 2002.

[1] Solute transport through highly heterogeneous geologic environments with connected pathways through high-conductivity material and lenses of low permeability often is not described well by a macroscopic advection-dispersion equation. An upscaled advection-dispersion model with a uniform velocity and dispersion coefficient does not predict the significant plume asymmetry and extended tailing often observed over finite distances in such environments. We investigate the hydrogeologic conditions under which an upscaled model must incorporate another mechanism to describe the extended tailing arising from slow advection through and diffusion into and out of low-permeability inclusions. We use high-resolution simulations to determine ground truth transport results for 84 hydrogeologic scenarios comprising distinct low-permeability lenses set into an otherwise homogeneous background. We compare the ability of two one-dimensional, fitted, upscaled models to reproduce the arrival time curves from the fully resolved simulations. The first model uses a macrodispersion coefficient to describe the spreading due to the low-permeability inclusions. The second model accounts for the effect of the geologic heterogeneity with a nonequilibrium mass transfer component. When the equivalent conductivity of a domain is less than or equal to the geometric mean conductivity, a macroscopic advection-dispersion model matches the results well. When the equivalent conductivity is greater than the geometric mean, however, another model may be needed to describe the solute tailing. *INDEX TERMS*: 1829 Hydrology: Groundwater hydrology; 1831 Hydrology: Groundwater quality; 1832 Hydrology: Groundwater transport; *KEYWORDS*: lenses, solute transport, equivalent conductivity, upscaling, modeling, heterogeneity

## 1. Introduction

[2] Efficient and effective solute transport simulation requires a model capable of describing the important characteristics of plume evolution, as defined by the objectives of the investigation. For many activities, the time for a contaminant or solute to be removed from a geologic environment is of particular interest. This characteristic depends strongly on the rate of solute elution from nearly stagnant regions that arise due to the heterogeneity of the hydraulic conductivity field. Since an explicit representation of all geologic variability is not feasible when simulating transport, the effects of the hydrogeologic heterogeneity must be captured with an upscaled model. This proves difficult for geologic environments with connected pathways through high-conductivity material and distinct regions of low permeability, which can lead to significant plume asymmetry and extended tailing.

[3] The observed concentration history or profile of a conservative solute is often not described well by a macroscopic advection-dispersion equation with a uniform

velocity and apparent dispersion coefficient. In some cases, the assumptions about the hydraulic conductivity underlying the application of stochastic theory, such as the log conductivity field being multi-Gaussian with small variance [cf. *Dagan*, 1989; *Gelhar*, 1993], may not be valid. In other cases, the scale of the transport problem may be too small, and the expected values of solute concentration predicted by stochastic theory cannot be compared directly with observations. Many have investigated the approach of the concentrations associated with a particular solute plume toward the expected values given by stochastic theory under various conditions [e.g., *Kapoor and Gelhar*, 1994; *Kapoor and Kitanidis*, 1996; *Pannone and Kitanidis*, 1999].

[4] To explore the utility of the stochastic theory of solute transport in a field setting, the Macrodispersion Experiment (MADE) was conducted in a heterogeneous aquifer near Columbus, Mississippi [*Boggs et al.*, 1992]. The alluvial aquifer in which this 20-month, natural-gradient, tracer study was performed is highly heterogeneous. The variance of the log conductivity field,  $\sigma_Y^2$ , is 4.5, and the horizontal and vertical integral scales are 12.8 and 1.6 meters, respectively [*Rehfeldt et al.*, 1992]. *Adams and Gelhar* [1992] observed that the resulting solute plume exhibited “dramatically non-Gaussian behavior,” and the longitudinal macro-

dispersivity estimated from the field measurements was about five times larger than the value predicted by the stochastic theory. For this field experiment, a macroscopic advection-dispersion equation describes the solute plume poorly.

[5] In addition to the work done on the MADE site, many others have explored the nature of solute spreading and the applicability of a macroscopic advection-dispersion equation in highly heterogeneous environments. For example, *Desbarats* [1987, 1990] investigated flow and advective transport through bimodal sandstone-shale sequences. With his three-dimensional numerical experiments, the author found that solute spreading departed significantly from Gaussian when there was a large contrast between the sand and shale conductivities. In these cases, the arrival of a conservative tracer at a downgradient location exhibited three behavior regimes: the early arrival of solute that did not travel through the shales, a middle period of almost no solute arriving at the plane of observation, and the late arrival, or tailing, of solute that passed through the shale bodies.

[6] *Moreno and Tsang* [1994] conducted numerical simulations of transport through conductivity fields with a range of variances. For the high-variance cases, flow was channeled through the high-permeability regions giving rise to the early arrival of solute peaks. *Jussel et al.* [1994a, 1994b] created a detailed model of a heterogeneous fluvial gravel deposit in northern Switzerland. The authors modeled transport through this environment and found that the predictions from stochastic theory did not match the observed solute spreading, due in part to the existence of coherent sedimentary structures [*Jussel et al.*, 1994b]. *Wen and Gómez-Hernández* [1998] performed a Monte Carlo analysis to investigate the effects of non-multi-Gaussian conductivity fields on transport. They considered four models of spatial variability for the hydraulic conductivity, all with the same univariate and two-point statistics, but with varying connectedness of extreme values. Transport through the non-multi-Gaussian conductivity fields differed significantly from the numerical and theoretical results for the multi-Gaussian case.

[7] Because of shortcomings such as these, many alternative models and enhancements to stochastic theories have been explored to describe anomalous transport behavior in heterogeneous environments. *Stauffer and Rauber* [1998] expanded on the theory developed by *Rubin* [1995] to derive macrodispersion coefficients for anisotropic, bimodal, permeability distributions. They simulated transport through realistic models of a three-dimensional, bimodal, glaciofluvial environment and compared macrodispersivity predictions from their theory to the simulated results. The theory did not accurately describe the apparent macrodispersivity determined from the simulations, overpredicting it at early times and underpredicting it at late time. *Berkowitz and Scher* [1998] and *Berkowitz et al.* [2000] used a continuous time random walk (CTRW) model to describe transport through complex geologic environments. This model was able to reproduce anomalous breakthrough curves from the MADE site [*Berkowitz and Scher*, 1998] and those from transport through a heterogeneous medium composed of low-permeability blocks set into a homogeneous background [*Berkowitz et al.*, 2000].

[8] Another popular method of enhancing the advection-dispersion equation has been to add a nonequilibrium mass transfer component, which accounts for the exchange of solute between regions of the domain conceptualized as mobile and immobile. Commonly, the mass transfer is represented with a linear driving force model [e.g., *Deans*, 1963; *Coats and Smith*, 1964], which gives rise to the following governing equations for transport:

$$\frac{\partial C_m}{\partial t} + \beta \frac{\partial C_{im}}{\partial t} = \nabla \cdot \mathbf{D} \nabla C_m - \mathbf{v}_m \cdot \nabla C_m \quad (1)$$

$$\frac{\partial C_{im}}{\partial t} = \alpha (C_m - C_{im}) \quad (2)$$

$$\beta = \frac{\theta_{im}}{\theta_m} \quad (3)$$

where  $C_m$  and  $C_{im}$  are the solute concentrations in the mobile and immobile phases,  $\theta_m$  and  $\theta_{im}$  are the volume fractions of the mobile and immobile phases,  $v_m$  is the average groundwater velocity through the mobile phase,  $D$  is the effective dispersion tensor, and  $\alpha$  is the rate of exchange between the mobile and immobile phases.

[9] *Harvey and Gorelick* [2000] used this model, with the dispersion set to zero, to describe the bromide and tritium plumes from the MADE site. They used the mass transfer component of the model to represent diffusion to and from low-permeability lenses at the centimeter to decimeter scale. This model described the asymmetry of the observed plume better than the macrodispersion model and predicted the overestimation of contaminant mass at early times and underestimation at late times [*Harvey and Gorelick*, 2000].

[10] Others have similarly tried to capture the anomalous effects of larger-scale geologic heterogeneity with mobile-immobile models. *Herr et al.* [1989] conducted laboratory experiments of tracer transport through columns packed with sand and either higher or lower permeability inclusions. For the experiments with the more permeable inclusions, the advection-dispersion equation described the data well. For the trials with lower-permeability inclusions, however, the ADE could not capture the tracer behavior, but the results were described well with a linear driving force model. *Bajracharya and Barry* [1997] accurately described tracer behavior in column experiments with centimeter-scale porous polyethylene cylinders embedded in sand and silt with a linear driving force model. Recently, *Zinn and Harvey* [2000] explored transport through non-multi-Gaussian conductivity fields with numerical simulations. Transport through domains with increased connectedness of high-conductivity material exhibited nonequilibrium mass transfer behavior.

[11] Though the mass transfer models were originally developed to describe rate-limited sorption processes or slow diffusion into and out of stagnant regions, *Guswa and Freyberg* [2000] demonstrated that anomalous tailing may also arise from slow advection through nearly stagnant regions. That work showed that the character of the tailing due to slow advection through a low-permeability lens differs only subtly from that due to diffusion and that knowledge of the first, second, and third temporal moments is not enough to distinguish between the two cases. Thus even in domains without truly stagnant zones, a mass transfer

formulation may successfully describe solute spreading when the advection-dispersion equation does not.

[12] The effect of geologic heterogeneity on solute spreading in some environments can be described by macrodispersion. In other cases, however, a more complex model is necessary. Efficient and effective simulation of solute transport requires knowing the circumstances under which an advection-dispersion model is adequate and those under which a different model is needed. We begin to answer this question with a modeling study of transport through environments containing connected paths through high-conductivity material and distinct low-permeability lenses.

## 2. Theoretical Considerations

[13] For environments with low-permeability inclusions embedded in a higher conductivity matrix, we would like to uncover those hydrogeologic conditions for which an upscaled advection-dispersion equation does not adequately describe solute transport. In such cases, improved performance can be achieved in a variety of ways, such as increasing the spatial resolution of the conductivity field or using one of a variety of alternative upscaled models. We focus on the improvement brought about by employing a mass transfer model to represent solute spreading; i.e., we look to identify when the improvement over the advection-dispersion equation warrants the use of a mobile-immobile model. Such a situation requires two conditions.

1. Regions of very low groundwater velocity exist in the domain such that the characteristic time for flow through these regions is long relative to the mean transport time through the domain [Guswa and Freyberg, 2000].

2. Transport through these regions is slow enough to affect significantly the bulk transport behavior. Satisfying the first condition automatically satisfies this second condition, if advection dominates transport within the lens. If diffusion dominates, the local equilibrium assumption may be applicable if the diffusion process is fast enough. In such a case, transport will be described well by an advection-dispersion equation (with coefficients modified by a retardation factor). A number of investigators have developed criteria for determining the importance of the kinetics of mass transfer via diffusion and the validity of the local equilibrium assumption [e.g., Valocchi, 1985; Bahr and Rubin, 1987; Cunningham, 1998].

[14] The first condition, which is a function of the flow regime alone, is a necessary but not sufficient condition for the need for a model that can represent extended tailing. The nature of this requirement implies that the characteristic time for advection through a single inclusion would provide a good measure of the possible need for a mass transfer model. This time scale, however, is difficult to determine; it requires knowledge of the size, shape, orientation, conductivity, and spatial arrangement of the low-permeability lenses [Guswa and Freyberg, 2000], and it is not applicable to environments without well-defined inclusions. Such limitations prompt the search for a simpler, more general criterion for determining the flow conditions under which a mass transfer model may be needed.

[15] We propose the normalized deviation of the equivalent hydraulic conductivity from the geometric mean con-

ductivity as such a criterion:

$$\Gamma = \frac{K_{eq} - K_G}{\sigma_K} \quad (4)$$

where  $K_G$  is the geometric mean and  $\sigma_K$  the standard deviation of the fully resolved hydraulic conductivity distribution.  $K_{eq}$  is the equivalent conductivity of the upscaled domain:

$$K_{eq} = \frac{Q}{AJ} \quad (5)$$

where  $Q$  is the volumetric flux through the domain,  $A$  is the cross-sectional area, and  $J$  is the imposed head gradient.

[16] Based on stochastic theory, the geometric mean conductivity is the equivalent conductivity of an infinite, two-dimensional, isotropic medium [Matheron, 1967]. If the hydrogeologic conditions are such that this conductivity predicted by stochastic theory is applicable, then so might be the apparent macrodispersivity. When investigating conductivity fields that are not multi-Gaussian, the deviation of the equivalent hydraulic conductivity from the geometric mean may serve as a surrogate measure of geologic structure to indicate whether or not an upscaled advection-dispersion equation alone is enough to describe solute transport.

[17] The use of the equivalent conductivity is also motivated by the work by Herr *et al.* [1989], who showed that transport through a domain comprising high-permeability lenses in a low-permeability matrix was adequately described by an advection-dispersion equation, while transport through a high-permeability matrix with low-permeability lenses required a mobile-immobile model. Due to the differences in connectedness of the high-permeability material, the equivalent conductivities of these domains differ; the equivalent conductivity of the former is less than the equivalent conductivity of the latter. Apparent macrodispersivities predicted by stochastic theory for these two environments are the same, however, given the same conductivity contrast and volume ratio of lenses to matrix [cf. Stauffer and Rauber, 1998], since the difference in geologic structure is in the connectedness, not the variance or integral scale of the conductivity field.

[18] Our hypothesis is that if the equivalent conductivity of a domain is less than or equal to the geometric mean conductivity (i.e.,  $\Gamma \leq 0$ ), then a macroscopic advection-dispersion equation is adequate; if  $\Gamma > 0$ , then a model incorporating mass transfer may be required. Exploring some limiting conditions gives further insight.

- If the conductivity field is homogeneous ( $\sigma_K = 0$ ), solute transport is described well by an advection-dispersion equation. In this case,  $\Gamma$  is strictly undefined, but for a lognormal hydraulic conductivity distribution,  $\Gamma$  goes to zero as  $\sigma_K$  approaches zero.

- If some fraction of the domain is truly impermeable, then regions of stagnant groundwater will exist. Since  $K_G = 0$  in this case,  $\Gamma$  will always be greater than zero (except in the degenerate case when  $K_{eq} = 0$ ). Accounting for the effects of the exchange of solute with the impermeable regions may require a mass transfer model, depending on the rate of diffusion into and out of the regions.

- When the equivalent conductivity is less than the geometric mean,  $\Gamma$  is less than zero. At the lower limit, the domain is stratified with flow perpendicular to the stratification, and the equivalent conductivity equals the harmonic mean. In this case, the groundwater velocity will be uniform if the porosity is constant. The heterogeneity of the conductivity field does not contribute to plume dispersion, and an advection-dispersion model will be adequate to describe solute transport.

- When the equivalent conductivity is greater than the geometric mean,  $\Gamma$  is greater than zero. At the upper limit, the domain is stratified with flow parallel to the layering, and the equivalent conductivity is equal to the arithmetic mean. In this case, the mean arrival time of an injected pulse of solute at a downgradient observation plane is

$$\mu_{1,layered} = \frac{L_t}{K_A J/n} \quad (6)$$

where  $L_t$  is the transport distance and  $n$  is the porosity (taken as uniform). For a binary formation, this becomes

$$\mu_{1,layered} = \frac{L_t}{[fK_i + (1-f)K_o]J/n} \quad (7)$$

where  $f$  is the fraction of the domain occupied by low-permeability material,  $K_i$  is the lower conductivity, and  $K_o$  is higher conductivity. Because of the infinite correlation of groundwater velocities in the direction of flow, an advection-dispersion equation with a constant dispersion coefficient is unable to describe a plume traveling through a perfectly stratified medium [Matheron and de Marsily, 1980]. Considering advection only, the variance of arrival times grows quadratically, rather than linearly, with distance. The second temporal moment resulting from advection through a stratified medium composed of two materials is

$$\mu_{2,layered} = \left(\mu_{1,layered}\right)^2 \frac{f(1-f)(K_i - K_o)^2}{K_i K_o} \quad (8)$$

If  $K_o \gg K_i$ , then (7) and (8) become

$$\mu_{1,layered} = \frac{L_t}{K_o J/n} (1 + \beta) \quad (9)$$

$$\mu_{2,layered} = \left(\frac{L_t}{K_o J/n}\right)^2 \beta \left(\frac{K_o}{K_i}\right) \quad (10)$$

where  $\beta = f/(1-f)$ . The moment expressions for a mobile-immobile model with no local dispersion, a mobile velocity equal to the velocity in the fast layer ( $K_o J/n$ ), and a characteristic time of mass transfer,  $t_i$ , equal to the time to advect through the slow layer ( $L_t/(K_i J/n)$ ), are

$$\mu_{1,MT} = \frac{L_t}{v_m} (1 + \beta) = \frac{L_t}{K_o J/n} (1 + \beta) \quad (11)$$

$$\mu_{2,MT} = \frac{L_t}{v_m} \beta t_i = \frac{L_t}{K_o J/n} \beta \frac{L_t}{K_i J/n} = \left(\frac{L_t}{K_o J/n}\right)^2 \beta \left(\frac{K_o}{K_i}\right) \quad (12)$$

In this case, the results for advection through a stratified medium are equal to those for the mobile-immobile model.

[19] The results for the limiting cases indicate that  $\Gamma$  should be a good indicator of the hydrogeologic conditions for which the advection-dispersion equation is adequate and those for which a mass transfer model may be needed. When  $\Gamma$  is less than or equal to zero, a macroscopic advection-dispersion equation should be sufficient. When  $\Gamma$  is greater than zero, however, the addition of another mechanism may be necessary to describe the solute tailing. As defined,  $\Gamma$  is a measure of the flow conditions alone and cannot be used to indicate the relative importance of diffusion. Consequently, a value of  $\Gamma$  greater than zero is not enough by itself to determine the need for a mobile-immobile model; one must also have insight into the significance of diffusion.

### 3. Methodology

[20] To determine the utility of  $\Gamma$ , we investigate the ability of two upscaled transport models with homogeneous coefficients to reproduce the breakthrough curves from highly resolved, ground truth simulations of transport through a variety of environments containing low-permeability lenses. The upscaled models employed are the traditional advection-dispersion model and the linear driving force model. We chose these two because the linear driving force model is a commonly used model that can represent extended solute tailing, and the advection-dispersion equation is the most frequently used model to describe the transport of a conservative solute. In order to focus on the differences in model structure, parameters of these models are chosen so that the predicted first and second temporal moments match those of the ground truth arrival time curves. The appropriateness of each model is determined by the overall fit of the arrival time curves from the upscaled models to those from the high-resolution simulations.

#### 3.1. Ground Truth Scenarios

[21] We consider 84 two-dimensional environments comprising homogeneous low-permeability lenses set into a homogeneous background material. Such environments might represent, for example, sandstone petroleum reservoirs with interbedded shales or near-surface aquifers composed of fluvial deposits. We use a square domain ( $L \times L$ ) and impose a macroscopic head gradient,  $J$ . Among the 84 scenarios, we vary the fraction of low-permeability material ( $f$ ), the relative size of the inclusions ( $a/L$ ), the eccentricity ( $a/b$ ) of the inclusions, the orientation of the lenses ( $\theta$ ) relative to the direction of the head gradient, and the contrast in hydraulic conductivity between the inclusions and the background material ( $K_i/K_o$ ). (For visual clarity and consistency, we have chosen to align the head gradient with the  $x$  axis in the simulations. The scenarios with lenses parallel to the head gradient will be readily distinguishable from those with the lenses perpendicular. Note that the  $x$  axis is not necessarily parallel to the ground surface.) Table 1 identifies the combinations of hydrogeologic conditions we investigate. All variables are defined in the Notation section.

[22] Indicator fields representing the inclusions and the background material are generated with the GSLIB application ellipsoid [Deutsch and Journel, 1992]. The geometric and hydrogeologic character of the individual inclusions is specified for each scenario, but the locations of the ellipses are chosen randomly with a pure nugget correlation struc-

**Table 1.** Parameter Values Used for Ground Truth Simulations

$f$	$K_l/K_o$	$a/L$	$a/b$	$\theta$
0.025	0.05	0.02	2, 8	0, 45, 90
0.025	0.05	0.04	2, 8	0, 45, 90
0.025	0.0005	0.02	2, 8	0, 45, 90
0.025	0.0005	0.04	2, 8	0, 45, 90
0.05	0.05	0.02	2, 8	0, 45, 90
0.05	0.05	0.04	2, 8	0, 45, 90
0.05	0.05	0.08	2, 8	0, 45, 90
0.05	0.0005	0.02	2, 8	0, 45, 90
0.05	0.0005	0.04	2, 8	0, 45, 90
0.05	0.0005	0.08	2, 8	0, 45, 90
0.10	0.05	0.02	2, 8	0, 45, 90
0.10	0.05	0.04	2, 8	0, 45, 90
0.10	0.05	0.08	2, 8	0, 45, 90
0.10	0.0005	0.04	2, 8	0, 45, 90

ture. To investigate and quantify the effects due to the specific locations of the lenses, five realizations are generated for each scenario. These five are not intended to fully characterize the variability among realizations, but to obtain some measure of the detail lost by upscaling and ignoring the detailed structure of the conductivity field.

[23] The indicator fields are scaled to match the two conductivity contrasts given in Table 1. This leads to 420 different geologic representations of the multiple inclusion environments. Figures 1 and 2 provide examples of the environments considered in this work. The left-hand plot provides an image of the conductivity distribution, and the semivariograms of  $\ln(K)$  for the  $x$  and  $z$  directions are plotted on the right-hand side.

[24] A block-centered, finite difference, numerical model for flow is applied over the  $400 \times 400$  grid of hydraulic conductivity values. With this resolution, the smallest inclusions, i.e., those from the scenarios with  $a/L = 0.02$  and  $a/b = 8$ , are approximately sixteen grid cells long and two cells wide. Constant head boundaries are imposed on the left and right sides of the model; no flow boundaries are imposed on the top and bottom. The background conductivity is set to a constant value,  $K_o$ , for all simulations, and a constant effective porosity,  $n$ , is assigned to the entire domain. For each simulation, the global mass balance error is less than 0.5 percent. To confirm the accuracy of the simulations, we compare the results for the six scenarios with the largest local and global mass balance errors to simulations with double the resolution ( $800 \times 800$ ); the results do not differ significantly from the  $400 \times 400$  simulations.

[25] We simulate two sets of transport processes through the highly resolved conductivity fields:

- Transport by advection only:  $Pe_b = Pe_d = \infty$ .
- Transport via advection and local dispersion, where the hydrodynamic dispersivities,  $\alpha_L$  and  $\alpha_T$ , and the effective diffusion coefficient,  $D_m$ , are uniform over the entire domain and the same for all scenarios:  $Pe_b = 3500$ ,  $Pe_d = 3500$ .

[26] The bulk Peclet number,  $Pe_b = L_l/\alpha_L$ , quantifies the relative strength of advection to mechanical dispersion, and the diffusion Peclet number,  $Pe_d = (K_o J \cdot L_l)/(nD_m)$ , quantifies the relative importance of advection to diffusion. In both cases, the bulk and diffusion Peclet numbers are large, indicating that the geologic heterogeneity will dominate the solute spreading. The Peclet number appropriate for an individual lens, which identifies the dominant transport

### Scenario 37, Realization 1

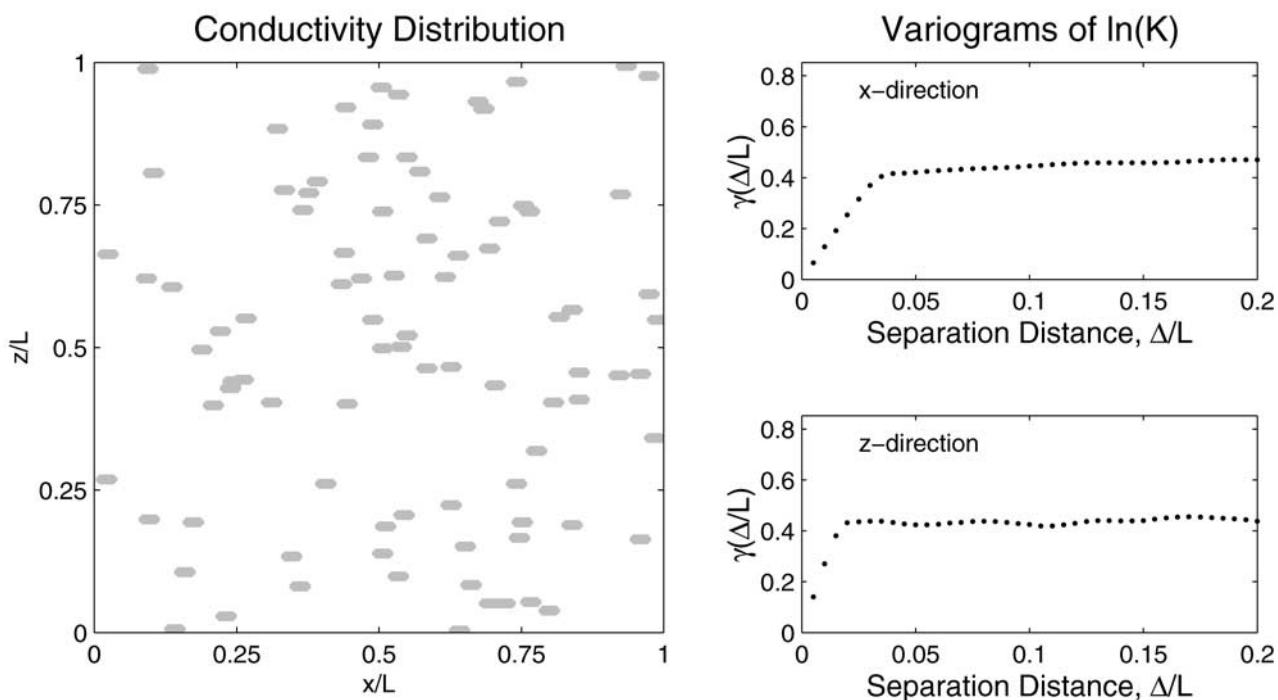


**Figure 1.** Hydraulic conductivity structure for scenario 37:  $f = 0.05$ ,  $K_l/K_o = 0.05$ ,  $a/L = 0.02$ ,  $a/b = 2$ ,  $\theta = 0^\circ$ . Right-hand plots present the experimental variograms for the  $x$  and  $z$  directions.

## Scenario 72, Realization 1

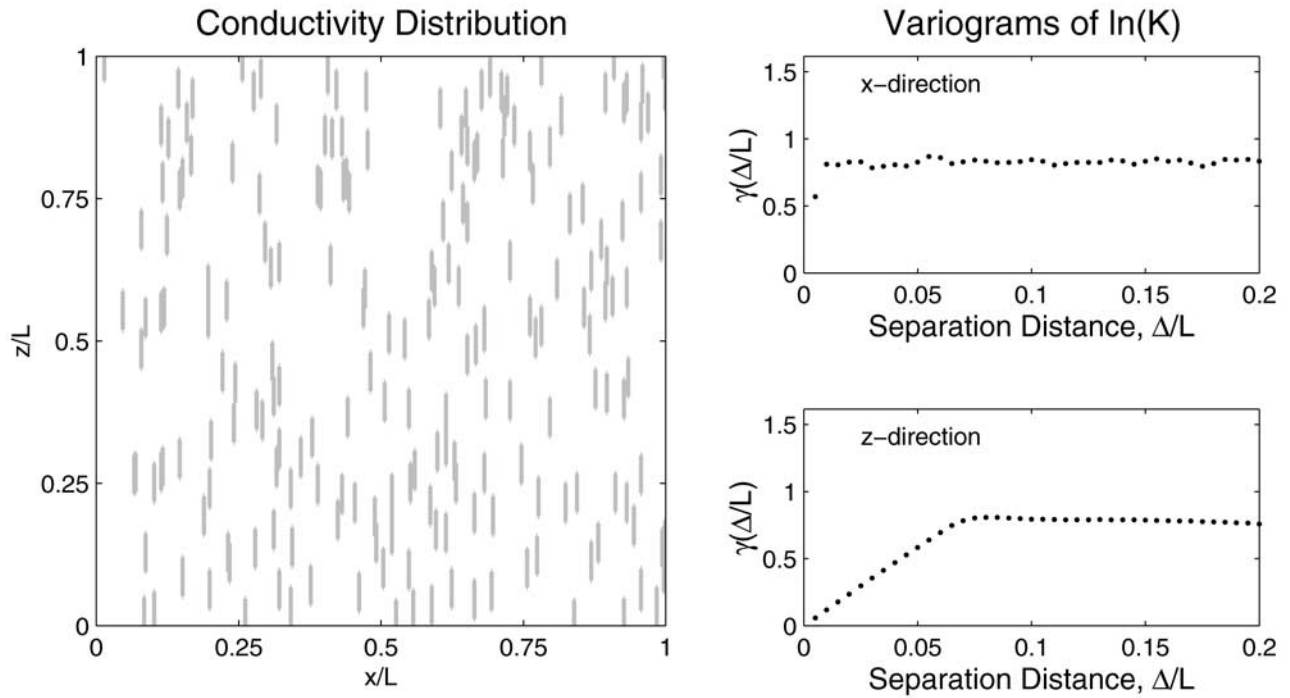


**Figure 2.** Hydraulic conductivity structure for scenario 72:  $f = 0.10$ ,  $K_i/K_o = 0.05$ ,  $a/L = 0.04$ ,  $a/b = 8$ ,  $\theta = 90^\circ$ . Right-hand plots present the experimental variograms for the  $x$  and  $z$  directions.

process within an inclusion (advection versus diffusion), depends on  $Pe_d$  along with the conductivity contrast and the specific geometry of the inclusion [Guswa and Freyberg, 2000]. Consequently, in some of the cases that include local dispersion, diffusion dominates transport to and from (and within) the inclusions because of their low permeability. These two sets of transport processes are chosen to compare behavior in the cases when advection dominates the transfer of solute to and from the lenses with cases when diffusion may be important.

[27] We simulate the transport of a conservative tracer by tracking approximately 40,000 particles through the domain. The particles are injected as a line extending over the full height of the domain at  $x/L = 0.05$  and tracked to an observation line at  $x/L = 0.925$ ; the total transport distance,  $L_t$ , is  $7/8$  the domain length. The initial distribution of particles along the line is weighted in proportion to the local flux.

[28] For transport via advection alone, we use a semi-analytical particle tracking scheme, described by Pollock [1989]. To simulate advection, dispersion, and diffusion, we use a random walk particle method [Uffink, 1985; Kinzelbach, 1990]. The particle velocities for advection are determined via linear interpolation from the interfacial velocities. This scheme is consistent with the block-centered, finite difference, flow model and has proven successful in the past [Goode, 1990; LaBolle et al., 1996]. Because of the abrupt variations in the hydraulic conductivity at the boundaries of the inclusions, we use bilinear interpolation to determine the velocities for the dispersion calculations, as suggested by LaBolle et al. [1996]. The time of first arrival at the downgradient control plane is

recorded for each particle, and the distribution of arrival times is used to create an arrival time curve for each simulation. To ensure that particles are not overaccumulating in the low-permeability lenses, we compare the mean particle arrival time for each simulation to the mean travel time determined from the corresponding flow simulation; normalized differences for all simulations are symmetrically distributed around zero with a standard deviation of less than one percent.

### 3.2. Upscaled Models

[29] We investigate the ability of two one-dimensional models, scaled up such that their coefficients are uniform, to describe the ground truth arrival time curves: (1) the macroscopic advection-dispersion model (ADE) with two parameters,  $v_{ADE}$  and  $D_{ADE}$ ; and (2) the linear driving force model (LDF) with four parameters,  $v_{MTB}$ ,  $D_{MTB}$ ,  $\beta$ , and  $\alpha$ .

[30] To investigate the appropriateness of the upscaled model structure, the model parameters are fit to reproduce the first and second temporal moments from the ground truth simulations. It is worth noting that the LDF model is an extension of the ADE model; the ADE model can be recovered from the LDF model by letting the capacity of the immobile phase go to zero. Thus, the LDF model can always perform as well or better than the ADE model if no restrictions are put on the determination of the parameters.

[31] Parameters of the ADE and LDF models are fit to reproduce the average of the first and second temporal moments of the arrival time curves for the five realizations of each scenario ( $\bar{\mu}_1$  and  $\bar{\mu}_2$ , respectively). For the advection-

dispersion model, specification of the first and second moments completely determines the parameters:

$$v_{ADE} = \frac{L_t}{\bar{\mu}_1} \quad (13)$$

$$D_{ADE} = \frac{\bar{\mu}_2 \cdot L_t^2}{2\bar{\mu}_1^3} \quad (14)$$

[32] Though the LDF model has four parameters, only two are fit: the velocity,  $v_{MT}$ , and the mass transfer rate,  $\alpha$ . Thus, the mobile-immobile model has the same number of fitted parameters as the ADE model, and it matches the same moments. The other parameters,  $\beta$  and  $D_{MT}$ , are determined a priori from quantities one may be able to estimate for a particular field application. The immobile capacity is set equal to the fraction of low-permeability material,  $f$ , and the mobile capacity to  $(1 - f)$ ; therefore  $\beta$  is given by

$$\beta = \frac{f}{1-f} \quad (15)$$

The velocity is determined from the first moment:

$$v_{MT} = \frac{L_t(1+\beta)}{\bar{\mu}_1} \quad (16)$$

The dispersion coefficient is set equal to the local longitudinal dispersivity used in the ground truth simulations times the velocity calculated in (16):

$$D_{MT} = \alpha_L \cdot v_{MT} \quad (17)$$

With this choice,  $D_{MT}$  accounts for the effects of local hydrodynamic dispersion but does not describe any of the additional spreading caused by the geologic heterogeneity. Instead, the LDF model accounts for that spreading with the nonequilibrium mass transfer process, and  $D_{MT}$  has very little effect on the transport. The mass transfer rate,  $\alpha$ , is chosen so that the average second temporal moment of the arrival time curves is reproduced for each scenario:

$$\alpha = \frac{2\beta}{(1+\beta)} \cdot \frac{\bar{\mu}_1}{(\bar{\mu}_2 - 2\bar{\mu}_1^2 \cdot \alpha_L/L_t)} \quad (18)$$

[33] With these parameters, both the ADE and LDF models reproduce the first and second temporal moments from the high-resolution transport simulations. Each will match the mean solute arrival time and the overall spread of solute observed in the ground truth simulations. The models account for the plume spreading resulting from the heterogeneous hydraulic conductivity field differently, however. The advection-dispersion model uses a macrodispersion coefficient, while the LDF model relies on a mass transfer process.

### 3.3. Model Evaluation Criteria

[34] We measure the lack of fit of the model predictions to the results of the numerical simulations with the quantiles (the  $j$ th quantile is the time of arrival of 100j percent of

the total solute mass) of the solute arrival time distributions:

$$\xi = \frac{1}{999} \sum_{i=1}^{999} \left( \ln \left[ \frac{q_{(i/1000)}^{model}}{\text{mean}(q_{(i/1000)}^{sim})} \right] \right)^2 \quad (19)$$

where  $q_{(i/1000)}^{model}$  is the quantile predicted by the one-dimensional upscaled model and  $\text{mean}(q_{(i/1000)}^{sim})$  is the mean quantile from the five realizations of each scenario. Thus, the results from the models are not compared to the arrival time curve from any one realization, but rather to a characteristic arrival time curve for the scenario. The criterion,  $\xi$ , indicates the overall lack of fit of the upscaled models to the simulations.

[35] The fitted model parameters are determined from the temporal moments, not  $\xi$ . therefore the values of  $\xi$  do not represent the minimum values possible. Rather, they reflect both the adequacy of the model structure and the method of fitting;  $\xi$  indicates how well a model that is designed to match the mean and variance of the arrival time distribution also matches the entire cumulative density function of the distribution. The parameter,  $\xi$ , enables us to determine which of the upscaled models better describes the ground truth arrival time curve. For a given scenario, a comparison of  $\xi$  between the two upscaled models determines which upscaled model is to be preferred. A comparison of  $\xi$  for the two models, however, does not provide any information about the goodness of fit in an absolute sense.

[36] The purpose of the upscaled models is to capture efficiently the basic character of the fully resolved results at the expense of the details of the ground truth simulations. In this study, the parameters for the upscaled models are fit based on average moments from the five realizations of each scenario, and the model predictions are compared to a characteristic arrival time curve for each scenario. One measure of the uncertainty associated with ignoring the realization-to-realization differences, is the variability in the arrival time curves among the realizations of a given scenario. To quantify this characteristic with a parameter that can be compared to  $\xi$ , we calculate  $\eta$ :

$$\eta = \frac{1}{999} \sum_{i=1}^{999} \left( \ln \left[ \frac{\max(q_{(i/1000)}^{sim})}{\min(q_{(i/1000)}^{sim})} \right] \right)^2 \quad (20)$$

This expression is a measure of the size of the envelope spanned by the arrival time curves from the five realizations for each scenario. A larger value of  $\eta$  indicates greater variability among the five realizations that compose each scenario. In our effort to find an upscaled model that captures the transport behavior of each scenario, a comparison of  $\xi$  with  $\eta$  indicates how well the upscaled model is reproducing that transport behavior relative to the inherent loss of information due to ignoring realization-to-realization variability.

## 4. Results

### 4.1. Illustrative Examples

[37] Figures 3 and 4 present two examples of the arrival time curves from transport simulations of advection only and the associated upscaled models. The left-hand plots

## Scenario 67

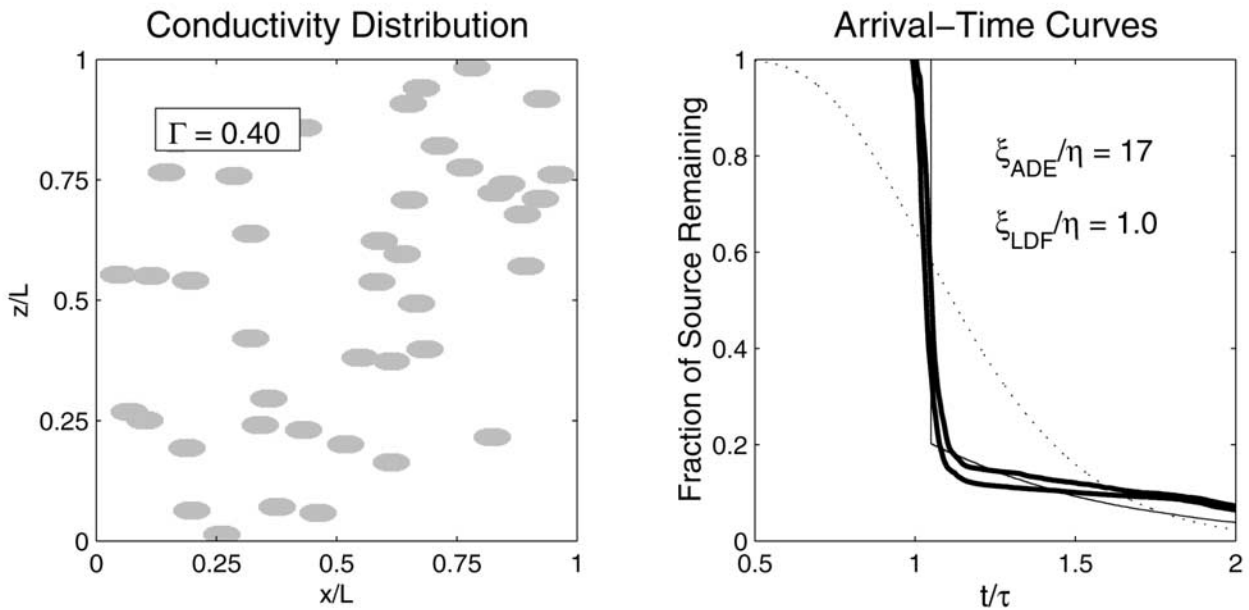


**Figure 3.** Example of simulated transport and associated model fits for scenario 67:  $f = 0.10$ ,  $K_i/K_o = 0.05$ ,  $a/L = 0.04$ ,  $a/b = 2$ ,  $\theta = 0^\circ$ . The left-hand plot presents an image of the conductivity field from one realization. The right-hand plot shows the envelope of ground truth arrival time curves for transport via advection only (thick solid lines), along with the fitted curves from the ADE (dotted line) and LDF (thin solid line) models.

## Scenario 11

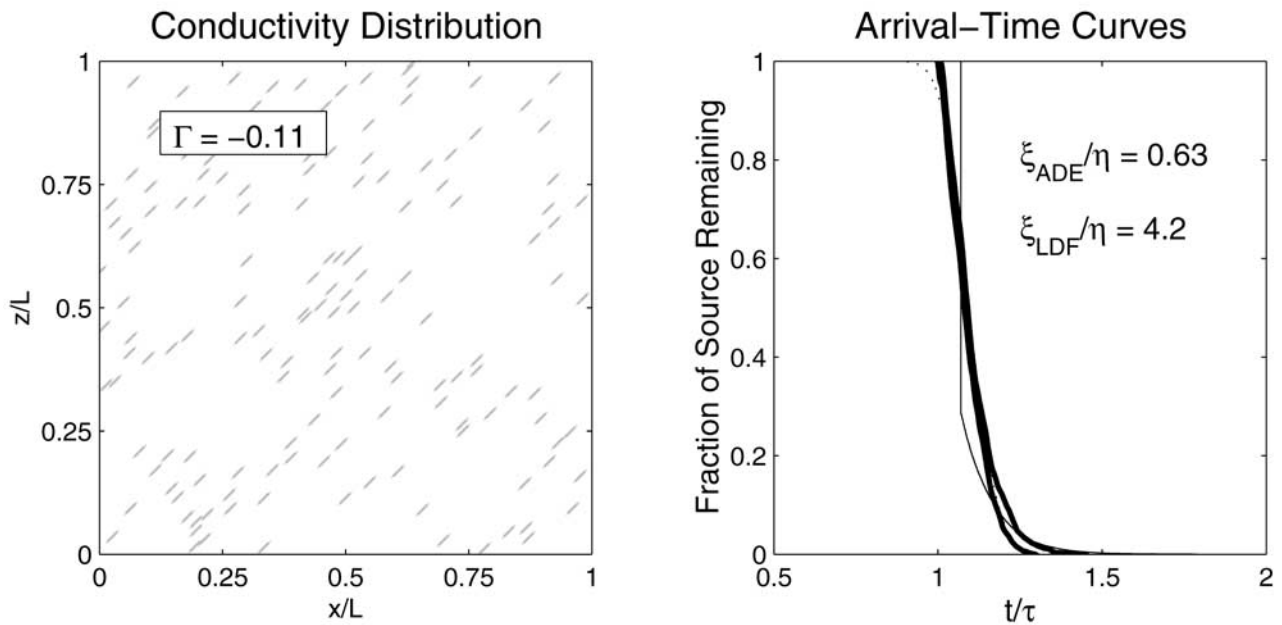


**Figure 4.** Example of simulated transport and associated model fits for scenario 11:  $f = 0.025$ ,  $K_i/K_o = 0.05$ ,  $a/L = 0.02$ ,  $a/b = 8$ ,  $\theta = 45^\circ$ . The left-hand plot presents an image of the conductivity field from one realization. The right-hand plot shows the envelope of ground truth arrival time curves for transport via advection only (thick solid lines), along with the fitted curves from the ADE (dotted line) and LDF (thin solid line) models.

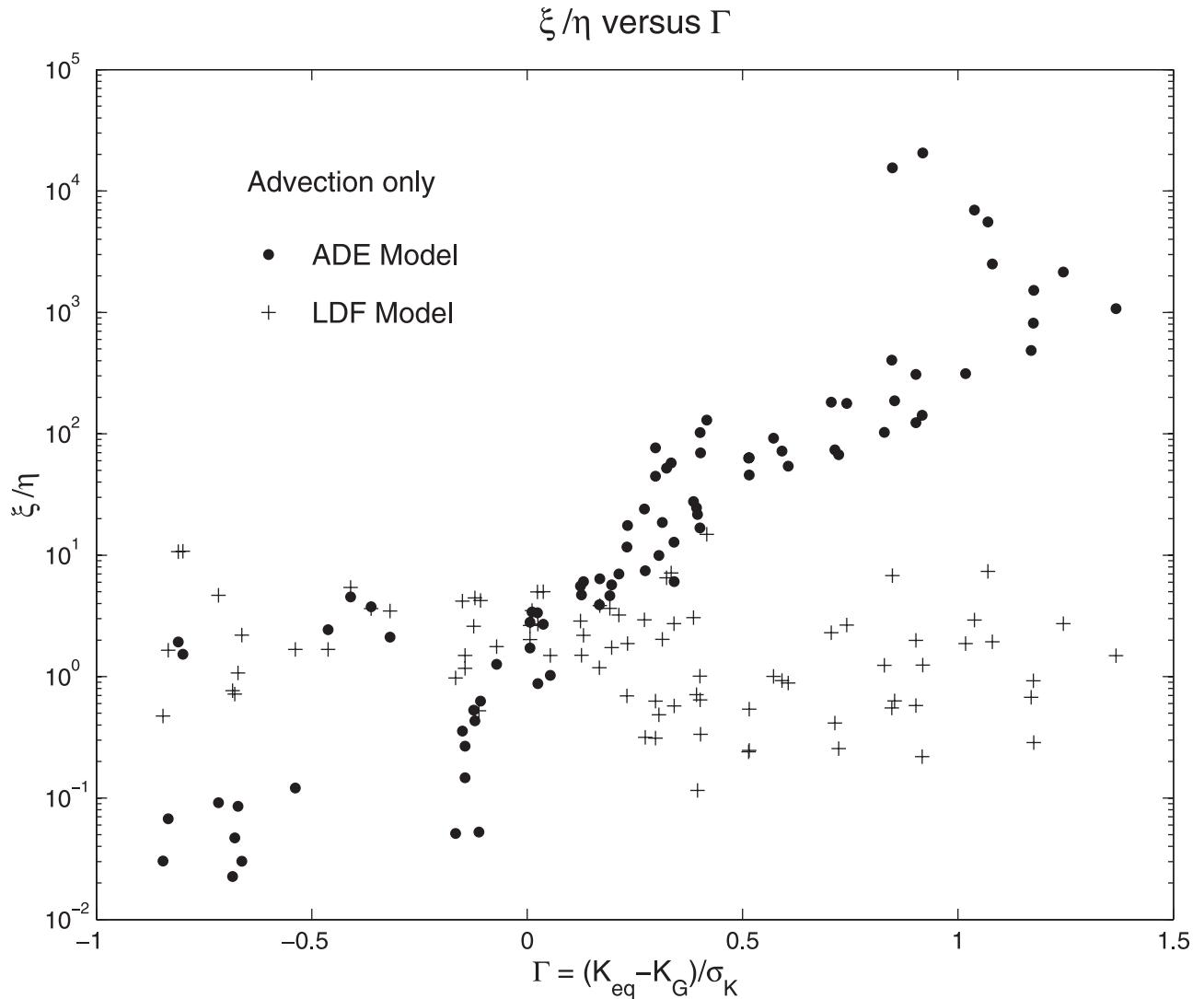


**Figure 5.** Comparison of the lack of fit of the ADE and LDF models to a measure of the variability among realizations for the ground truth simulations of advection only, plotted as a function of  $\Gamma$ .

present images of the hydraulic conductivity distribution. The right-hand plots show three arrival time curves: the heavy solid lines provide the envelope spanned by the ground truth curves from the particle-tracking simulations, the light solid line shows the curve produced by the linear driving force model, and the dotted line gives the result from the advection-dispersion equation. For the example given in Figure 3, the equivalent conductivity is greater than the geometric mean conductivity, and  $\Gamma$  equals 0.40. As anticipated, under these conditions the LDF gives a better fit to the arrival time curve from the simulation:  $\xi_{LDF}/\eta = 1.0$ ,  $\xi_{ADE}/\eta = 17$ . The lack of fit of the LDF model is comparable to the variability among the ground truth realizations. Note, however, that the tailing is not matched exactly, and the slight dispersion in the early arrivals for the ground truth simulations is not seen in the upscaled model result. Overall, though, the LDF model captures the character of the arrival time curves from the ground truth simulations.

[38] Figure 4 presents results for a contrasting example. The lenses are inclined with respect to the dominant flow

direction, and the inclusions are smaller, occupy less of the domain, and have a larger aspect ratio. The equivalent conductivity is less than the geometric mean conductivity,  $\Gamma = -0.11$ . The right-hand plot shows that the advection-dispersion equation fits the simulation results better than the linear driving-force model:  $\xi_{ADE}/\eta = 0.63$ ,  $\xi_{LDF}/\eta = 4.2$ . The arrival time curve for the ADE lies almost directly on top of the ground truth curves.

[39] Since there is no local dispersion in either of these examples (these ground truth simulations include advection only), the solute spreading is due entirely to the heterogeneity in the hydraulic conductivity field. In the first example, the character of the spreading is similar to the effects of a nonequilibrium mass transfer process. In the second example, the behavior is closer to the prototypical macrodispersion.

#### 4.2. Summary of Results for Advection Only

[40] Plots of  $\xi$  versus  $\Gamma$  summarize the ability of the upscaled models to reproduce the behavior of the advection-only simulations. Figure 5 presents  $\xi/\eta$  versus  $\Gamma$  for the

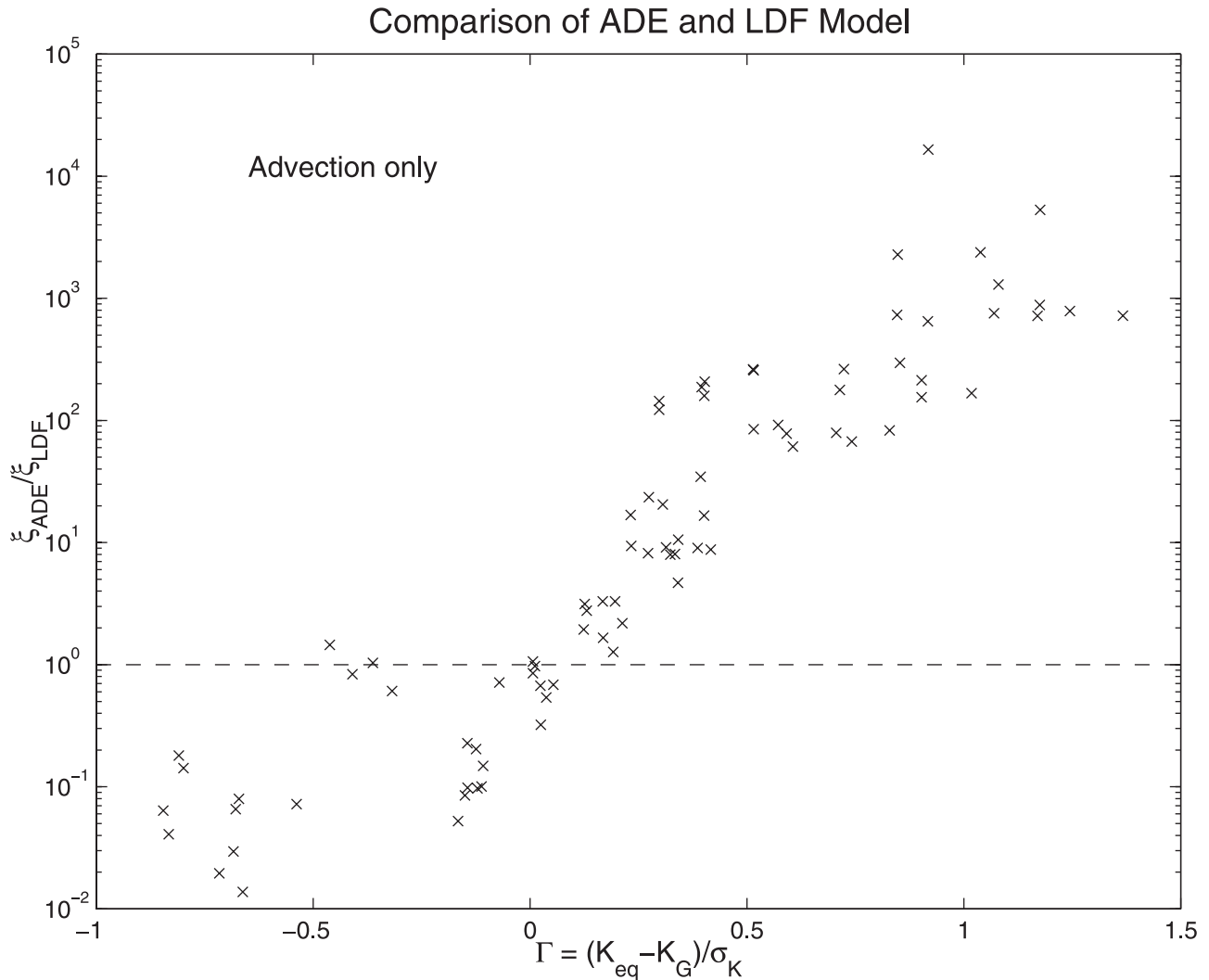


**Figure 6.** Comparison of the lack of fit of the ADE model to the LDF model for the ground truth simulations of advection only, plotted as a function of  $\Gamma$ . The dashed line indicates  $\xi_{ADE}/\xi_{LDF} = 1$ .

ADE (dots) and the LDF (pluses) models. Figure 5 shows that  $\xi/\eta$  for the LDF model ranges from 0.1 to 10 with little or no variation with  $\Gamma$ . For the ADE model, however,  $\xi/\eta$  ranges from 0.01 to 10,000 with a strong dependence on  $\Gamma$ . When  $\Gamma$  is less than or equal to zero, the lack of fit of the ADE to the simulations for each scenario is comparable to the variability among the realizations. For  $\Gamma$  greater than zero, however, the fit of the ADE to the simulation results is poor and gets worse as  $\Gamma$  increases. This plot indicates that reasonable results could be obtained with the LDF model for any value of  $\Gamma$ ; however, when  $\Gamma < 0$ , the ADE performs at least as well.

[41] Figure 6 compares  $\xi_{ADE}$  to  $\xi_{LDF}$  as a function of  $\Gamma$ . Since  $\xi$  is a measure of the lack of fit, a value of  $\xi_{ADE}/\xi_{LDF}$  greater than one implies that the fit of the LDF model is better than the ADE. The opposite is true for values of  $\xi_{ADE}/\xi_{LDF}$  less than one. From Figure 6, one can see that the breakpoint is close to  $\Gamma = 0$ . When  $\Gamma$  is greater than zero, the LDF model outperforms the ADE; when  $\Gamma$  is less than zero, the ADE does as well or better. One cluster of interesting scenarios are the four that give rise to a value of  $\Gamma \approx -0.4$  and  $\xi_{ADE}/\xi_{LDF} \approx 1.0$ . These scenarios are characterized by

large, eccentric, very low permeability inclusions, oriented perpendicular to the imposed head gradient. The models give comparable results because the tortuous nature of the flow paths around the lenses produces spreading that is described well by the ADE and the transport through the lenses gives rise to tailing that is captured by the LDF model.

#### 4.3. Summary of Results for Advection and Local Dispersion

[42] So far, we have focused on matching the results for the ground truth transport simulations incorporating advection only. In the simulations of advection and local dispersion, diffusion may dominate the transport through the low-permeability lenses. Since the flow conditions are identical for the two sets of transport simulations, the effect of diffusion is to speed up the transfer of solute to and from the low-permeability regions. Thus, diffusion can act to mix out the stretching and distortion of the plume caused by the advective variability. Since  $\Gamma$  is a measure of the hydrogeologic conditions only, it is independent of the strength of the local dispersion and does not measure the importance of diffusion as a transport process.

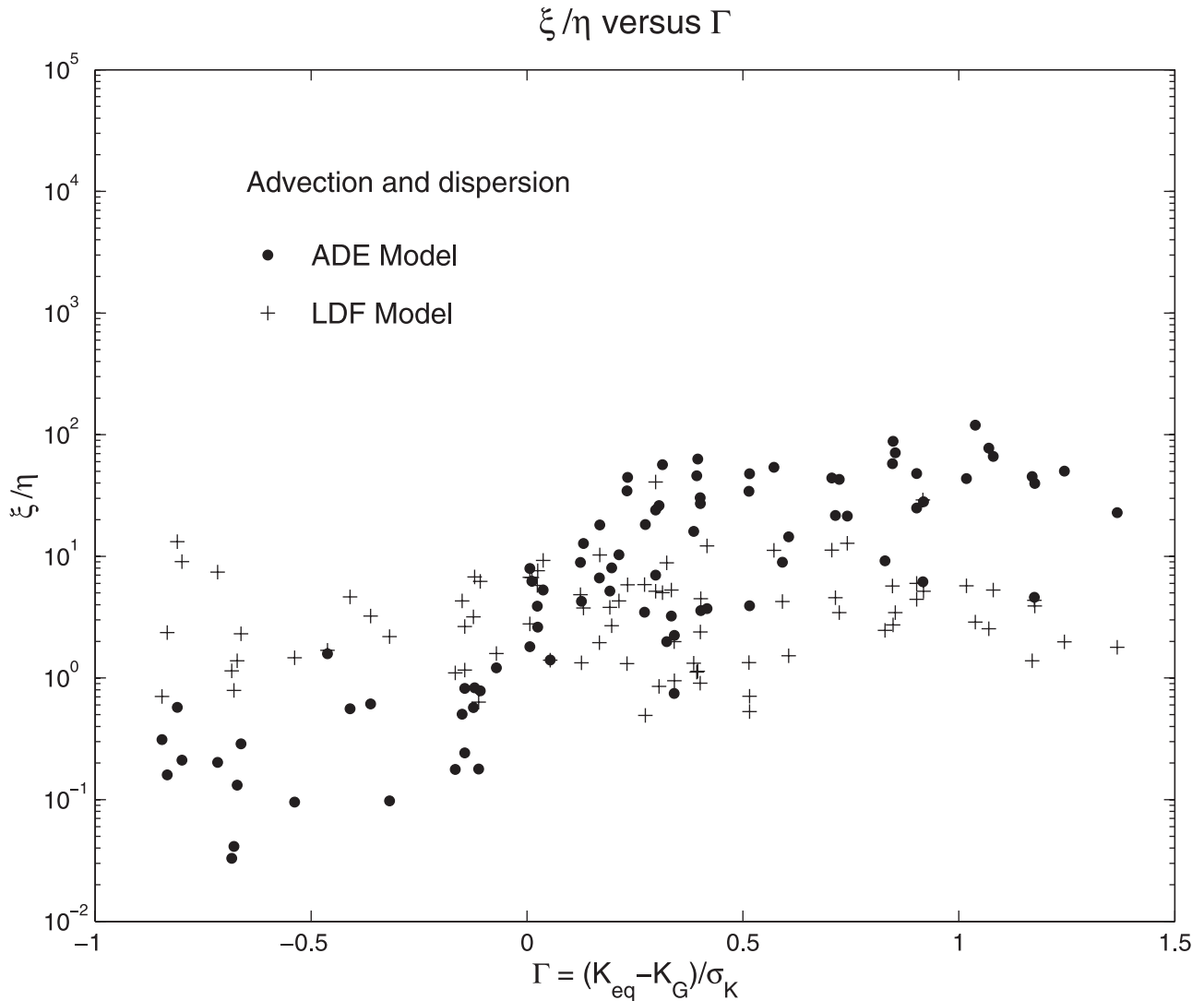


**Figure 7.** Comparison of the lack of fit of the ADE and LDF models to a measure of the variability among realizations for the ground truth simulations of advection and local dispersion, plotted as a function of  $\Gamma$ .

[43] Figure 7 presents the fit of the ADE (dots) and LDF (pluses) models to the ground truth simulations incorporating advection and local dispersion as a function of  $\Gamma$ . In Figure 7, the values of  $\xi/\eta$  for the LDF model are slightly larger than in Figure 5, but there is little variation with  $\Gamma$ , as before. The dependence of  $\xi/\eta$  on  $\Gamma$  for the advection-dispersion model is apparent, but it is not as pronounced as in Figure 5.

[44] Figure 8 shows the comparison of  $\xi_{ADE}$  with  $\xi_{LDF}$ . Again,  $\Gamma = 0$  appears to be a breakpoint, but the distinction is not as strong as in Figure 6. In Figure 8, there are some scenarios for which  $\xi_{ADE}/\xi_{LDF}$  is less than one when  $\Gamma$  is greater than zero. The characteristic times for advection and diffusion through an individual lens in these cases offer an explanation for this. For the scenarios highlighted by circles in Figure 8, the characteristic time for advection through a single lens is at least ten times longer than the characteristic time for diffusion. In these cases, diffusion acts to mix out the tailing that would otherwise arise under advection alone,

and, in some instances, this mixing obviates the need for a model other than the ADE.

## 5. Discussion

[45] The comparison undertaken here has looked at the utility of  $\Gamma$  as an indicator of the ability of two upscaled models, the ADE and the LDF, to reproduce the arrival time behavior of a solute traversing a domain with low-permeability inclusions. In the first model, a macrodispersion coefficient accounts for the effect of geologic heterogeneity on solute spreading. The second model uses a nonequilibrium exchange of solute between mobile and immobile phases to describe the solute spreading.

[46] The parameter  $\Gamma$  represents a measure of the flow conditions, incorporating the effects of the conductivity contrast, domain boundaries, and the orientation, size, and shape of the low-permeability lenses. When transport through all parts of the domain is dominated by advection,

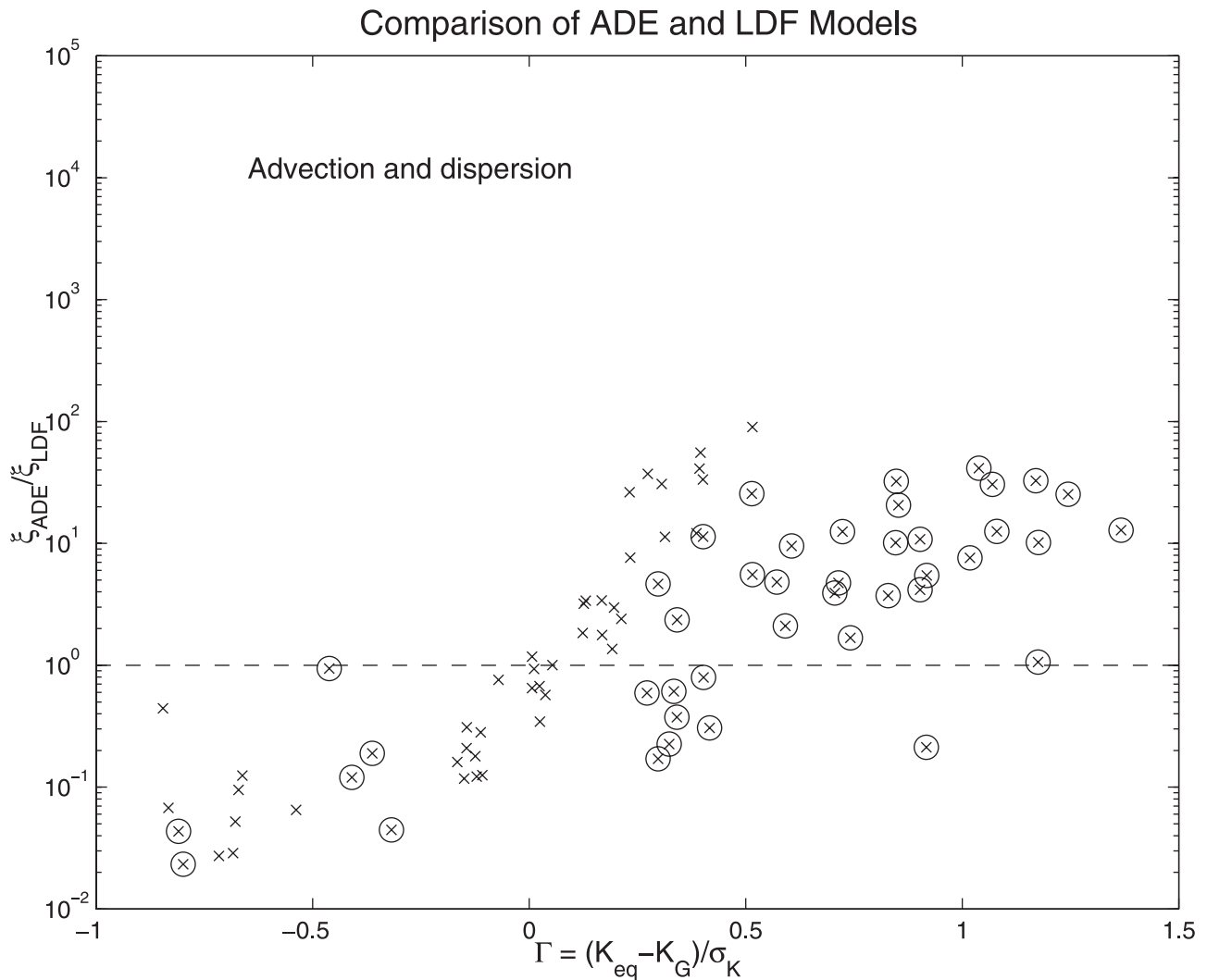


**Figure 8.** Comparison of the lack of fit of the ADE model to the LDF model for the ground truth simulations of advection and local dispersion, plotted as a function of  $\Gamma$ . Circles highlight those simulations for which the characteristic time for advection through a single lens is at least ten times longer than the characteristic time for diffusion. The dashed line indicates  $\xi_{ADE}/\xi_{LDF} = 1$ .

$\Gamma$  is sufficient to identify the utility of the ADE. When  $\Gamma$  is less than or equal to zero, an upscaled advection-dispersion equation alone can describe the evolution of a plume. If  $\Gamma$  is greater than zero, however, an additional component is needed to account for the tailing arising from sequestration of solute in the low-velocity regions. This need stems from the finite size of the domain; as the domain size grows, the equivalent conductivity will approach the geometric mean conductivity and the applicability of the ADE will improve.

[47] If diffusion plays an important role in the transport of solute through the low-velocity regions, a value of  $\Gamma$  less than zero still indicates that use of the ADE is appropriate. A value of  $\Gamma$  greater than zero, however, is not enough by itself to determine the need for another model.  $\Gamma$  is a measure of the flow conditions only and cannot account for the importance of diffusion. If the characteristic time for diffusion is short enough, plume separations due to advective variability will be mixed out, and solute spreading may be described adequately by an advection-dispersion equation. The criteria indicating the need for a nonequilibrium mass transfer model

to account for the diffusion of solute to and from an immobile zone have been well explored [e.g., *Valocchi, 1985; Bahr and Rubin, 1987; Cunningham, 1998*].

[48] The scenarios investigated in this work are an extreme subset of possible geologic environments, designed to represent environments with connected high-conductivity pathways and distinct regions of low permeability. The domains are two-dimensional and are composed of two materials with specific geometric arrangements. A review of previous work gives some insight to the applicability of the findings of this paper to other geologic conditions.

[49] *Desbarats* [1987, 1990] investigated flow and transport through sand-shale sequences, environments similar to those considered in this paper. His numerical experiments, however, covered a wider range of variation in the fraction of low-permeability material. For two- and three-dimensional isotropic media, the equivalent conductivity determined from his flow simulations was greater than the geometric mean conductivity for shale fractions less than 0.4 (in the 2D cases) and less than 0.65 (for the 3D cases);

across these thresholds, the equivalent conductivity dropped dramatically to a value below the geometric mean conductivity [Desbarats, 1987]. Advective transport was simulated through three-dimensional domains with shale fractions ranging from approximately five to fifty-five percent, and the results show extended tailing that could not be described with an advection-dispersion equation [Desbarats, 1990]. In these cases, the equivalent conductivity is greater than the geometric mean, and the results are consistent with the conclusions presented here. Since the maximum fraction of low-permeability material considered in these transport simulations is less than 0.65, however, the transport behavior for hydrogeologic conditions when the equivalent conductivity is less than the geometric mean conductivity, i.e., when  $\Gamma$  is less than zero, could not be determined.

[50] Berkowitz and Scher [1998] and Harvey and Gorelick [2000] found that alternatives to the macrodispersion model were needed to describe the evolution of the tritium and bromide plumes at the MADE site. The aquifer in which the tracer study was conducted is highly heterogeneous with a significant fraction of low-permeability material. Harvey and Gorelick [2000] estimated the geometric mean conductivity from small-scale permeameter and borehole flow meter measurements to be  $1.8 \times 10^{-4}$  cm/s. The flow field converges through the domain and the hydraulic head gradient is far from uniform. Even so, a rough estimate of the equivalent conductivity of the domain indicates that it is larger than the geometric mean conductivity. Therefore the need for a model beyond the advection-dispersion equation is not surprising.

[51] Zinn and Harvey [2000] investigated flow and transport through non-Gaussian random fields, and they found that transport through environments with connected pathways through high-conductivity material exhibited nonequilibrium mass transfer behavior. They also found that the equivalent conductivity for these environments was greater than the geometric mean conductivity. Environments without the connected paths through the high-conductivity material did not show extended tailing behavior.

[52] The above work indicates that  $\Gamma$  may characterize effectively the flow conditions in many environments. Part of the attractiveness of using  $\Gamma$  as an indicator is that it incorporates the effects of boundary conditions as well as the nature of the geology. This makes the quantity difficult to determine in the field, however. Surrogates for  $\Gamma$  can be determined by examining measurements of hydraulic conductivity with different support volumes. For example, comparing the distribution of hydraulic conductivity values measured with borehole flow meter tests to those from large-scale pump tests may provide an estimate of  $\Gamma$ . If such field measurements are not available,  $\Gamma$  may still be a valuable tool in transport modeling. Often the output from geostatistical models is too highly resolved to use directly in flow and transport simulations. The conductivity values for the upscaled blocks may be determined by simulating flow through the subdomains [Wen and Gómez-Hernández, 1996]. In such cases, one could use the flow results to determine if an advection-dispersion equation alone is adequate for transport within the upscaled blocks, or if another model may be needed.

[53] While knowledge of  $\Gamma$  may indicate the need for a model more sophisticated than the advection-dispersion

equation, one still needs a way to estimate the model parameters. With well-defined, regular inclusions, such as those in this work, this task is tractable [cf. Guswa, 2000]. More complex environments, however, present significant challenges to this endeavor, which are further complicated when the mass transfer behavior arises as a result of slow advection. In such cases, the mass transfer parameters will depend on the magnitude and direction of the hydraulic head gradient. This reduces the applicability of model parameters determined from a specific field or laboratory experiment. Developing general scaling relationships for such cases presents an opportunity for future exploration and research.

## 6. Conclusions

[54] We compare the ability of two one-dimensional, fitted, upscaled models to reproduce the arrival time curves from fully resolved simulations of transport through a variety of hydrogeologic scenarios comprising distinct low-permeability lenses set into a homogeneous background. The first model uses a macrodispersion coefficient to describe the spreading effects of the low-permeability inclusions, whereas the second model accounts for the effect of the geologic heterogeneity on solute spreading with a nonequilibrium mass transfer component. When the equivalent conductivity of a domain is less than or equal to the geometric mean conductivity, a macroscopic advection-dispersion model matches the results well. When the equivalent conductivity is greater than the geometric mean, however, another model may be needed to describe the solute tailing, depending on the importance of diffusion.

## Notation

$a$	semimajor axis of the elliptical inclusions [ $L$ ].
$b$	semiminor axis of the elliptical inclusions [ $L$ ].
$C_{im}$	solute concentration in the immobile phase [ $M/L^3$ ].
$C_m$	solute concentration in the mobile phase [ $M/L^3$ ].
$\mathbf{D}$	effective dispersion tensor [ $L^2/T$ ].
$D_m$	effective diffusion coefficient [ $L^2/T$ ].
$f$	fraction of domain composed of low-permeability material [—].
$J$	imposed hydraulic head gradient [—].
$K_A$	arithmetic mean of a conductivity distribution [ $L/T$ ].
$K_G$	geometric mean of a conductivity distribution [ $L/T$ ].
$K_i$	hydraulic conductivity inside an inclusion [ $L/T$ ].
$K_o$	hydraulic conductivity of the background material [ $L/T$ ].
$L$	size of the domain ( $L \times L$ ) [ $L$ ].
$L_t$	distance from injection to observation line [ $L$ ].
$n$	effective porosity [—].
$Pe_b$	Peclet number for transport through the background material [—].
$Pe_d$	diffusion Peclet number, quantifying the relative strength of advection to diffusion across the domain [—].
$q_j$	$j^{\text{th}}$ quantile of an arrival time distribution [ $T$ ].

- $t_i$  characteristic time for mass transfer,  $t_i = 2/\alpha$  for the LDF model [ $T$ ].
- $\mathbf{v}_m$  mobile-phase velocity [ $L/T$ ].
- $\alpha$  mass transfer parameter for the LDF model [ $1/T$ ].
- $\alpha_L$  longitudinal dispersivity [ $L$ ].
- $\alpha_T$  transverse dispersivity [ $L$ ].
- $\beta$  ratio of the immobile to mobile volume fraction [—].
- $\Gamma$  measure of hydrogeologic conditions [—].
- $\eta$  measure of the variability in arrival time curves among realizations [—].
- $\theta$  orientation of lenses; angle with respect to the  $x$  axis [ $^\circ$ ].
- $\theta_{im}$  volume fraction of the immobile phase [—].
- $\theta_m$  volume fraction of the mobile phase [—].
- $\mu_1$  first temporal moment of solute arrival, indicating the mean arrival time [ $T$ ].
- $\mu_2$  second, central, temporal moment of solute arrival, indicating the variance of arrival times [ $T^2$ ].
- $\bar{\mu}_i$  average  $i$ th temporal moment from the five realizations [ $T^i$ ].
- $\mu_i, \text{layered}$   $i$ th temporal moment for a layered medium [ $T^i$ ].
- $\mu_i, MT$   $i$ th temporal moment for a mobile-immobile model [ $T^i$ ].
- $\xi$  measure of the lack of fit of an upscaled model to the ground truth [—].
- $\sigma_K$  standard deviation of a conductivity distribution [ $L/T$ ].
- $\tau$  mean travel time for advection through the background material [ $T$ ].

## References

- Adams, E. E., and L. W. Gelhar, Field study of dispersion in a heterogeneous aquifer, 2, Spatial moment analysis, *Water Resour. Res.*, 28(12), 3293–3307, 1992.
- Bahr, J. M., and J. Rubin, Direct comparison of kinetic and local equilibrium formulations for solute transport affected by surface reactions, *Water Resour. Res.*, 23(3), 438–452, 1987.
- Bajracharya, K., and D. A. Barry, Non-equilibrium solute transport parameters and their physical significance: Numerical and experimental results, *J. Contam. Hydrol.*, 24, 185–204, 1997.
- Berkowitz, B., and H. Scher, Theory of anomalous chemical transport in random fracture networks, *Phys. Rev. E*, 57(5), 5858–5869, 1998.
- Berkowitz, B., H. Scher, and S. E. Silliman, Anomalous transport in laboratory-scale, heterogeneous porous media, *Water Resour. Res.*, 36(1), 149–158, 2000.
- Boggs, J. M., S. C. Young, L. M. Beard, L. W. Gelhar, K. R. Rehfeldt, and E. E. Adams, Field study of dispersion in a heterogeneous aquifer, 1, Overview and site description, *Water Resour. Res.*, 28(12), 3281–3291, 1992.
- Coats, K. H., and B. D. Smith, Dead-end pore volume and dispersion in porous media, *Soc. Pet. Eng. J.*, 4(1), 73–84, 1964.
- Cunningham, J. A., Sorption and desorption of organic contaminants by aquifer solids: Mechanisms, rates, and implications for transport in groundwater, Ph.D. thesis, Stanford Univ., Stanford, Calif., 1998.
- Dagan, G., *Flow and Transport in Porous Formations*, Springer-Verlag, New York, 1989.
- Deans, H. A., A mathematical model for dispersion in the direction of flow in porous media, *Soc. Pet. Eng. J.*, 3(1), 49–52, 1963.
- Desbarats, A. J., Numerical estimation of effective permeability in sand-shale formations, *Water Resour. Res.*, 23(2), 273–286, 1987.
- Desbarats, A. J., Macrodispersion in sand-shale sequences, *Water Resour. Res.*, 26(1), 153–163, 1990.
- Deutsch, C. V., and A. G. Journel, *GSLIB Geostatistical Software Library and User's Guide*, Oxford Univ. Press, New York, 1992.
- Gelhar, L. W., *Stochastic Subsurface Hydrology from Theory to Applications*, Prentice-Hall, Old Tappan, N. J., 1993.
- Goode, D. J., Particle velocity interpolation in block-centered finite difference groundwater flow models, *Water Resour. Res.*, 26(5), 925–940, 1990.
- Guswa, A. J., Modeling solute transport: Tailing due to low-permeability lenses, Ph.D. thesis, Stanford Univ., Stanford, Calif., 2000.
- Guswa, A. J., and D. L. Freyberg, Slow advection and diffusion through low permeability inclusions, *J. Contam. Hydrol.*, 46(3–4), 205–232, 2000.
- Harvey, C. F., and S. M. Gorelick, Rate-limited mass transfer or macrodispersion: Which dominates plume evolution at the macrodispersion experiment (MADE) site?, *Water Resour. Res.*, 36(3), 637–650, 2000.
- Herr, M., G. Schafer, and K. Spitz, Experimental studies of mass transport in porous media with local heterogeneities, *J. Contam. Hydrol.*, 4, 127–137, 1989.
- Jussel, P., F. Stauffer, and T. Dracos, Transport modeling in heterogeneous aquifers, 1, Statistical description and numerical generation of gravel deposits, *Water Resour. Res.*, 30(6), 1803–1817, 1994a.
- Jussel, P., F. Stauffer, and T. Dracos, Transport modeling in heterogeneous aquifers, 2, Three-dimensional transport model and stochastic numerical tracer experiments, *Water Resour. Res.*, 30(6), 1819–1831, 1994b.
- Kapoor, V., and L. W. Gelhar, Transport in three-dimensionally heterogeneous aquifers, 2, Predictions and observations of concentration fluctuations, *Water Resour. Res.*, 30(6), 1789–1801, 1994.
- Kapoor, V., and P. K. Kitanidis, Concentration fluctuations and dilution in two-dimensionally periodic heterogeneous porous media, *Transp. Porous Media*, 22, 91–119, 1996.
- Kinzelbach, W., Simulation of pollutant transport in groundwater with the random walk method, *IAHS Publ.*, 173, 265–279, 1990.
- LaBolle, E. M., G. E. Fogg, and A. F. B. Tompson, Random-walk simulation of transport in heterogeneous porous media: Local mass-conservative problem and implementation methods, *Water Resour. Res.*, 32(3), 583–593, 1996.
- Matheron, G., *Éléments pour une théorie des milieux poreux*, Masson, Paris, 1967.
- Matheron, G., and G. de Marsily, Is transport in porous media always diffusive? A counterexample, *Water Resour. Res.*, 16(5), 901–917, 1980.
- Moreno, L., and C.-F. Tsang, Flow channeling in strongly heterogeneous porous media: A numerical study, *Water Resour. Res.*, 30(5), 1421–1430, 1994.
- Pannone, M., and P. K. Kitanidis, Large-time behavior of concentration variance and dilution in heterogeneous formations, *Water Resour. Res.*, 35(3), 623–634, 1999.
- Pollock, J., Documentation of computer programs to compute and display pathlines using results from the U.S. Geological Survey modular three-dimensional finite-difference groundwater flow model, *U.S. Geol. Surv. Open File Rep.*, 89-381, 1989.
- Rehfeldt, K. R., J. M. Boggs, and L. W. Gelhar, Field study of dispersion in a heterogeneous aquifer, 3, Geostatistical analysis of hydraulic conductivity, *Water Resour. Res.*, 28(12), 3309–3324, 1992.
- Rubin, Y., Flow and transport in bimodal heterogeneous formations, *Water Resour. Res.*, 31(10), 2461–2468, 1995.
- Stauffer, F., and M. Rauber, Stochastic macrodispersion models for gravel aquifers, *J. Hydraul. Res.*, 36(6), 885–896, 1998.
- Uffink, G. J. M., A random walk method for the simulation of macrodispersion in a stratified aquifer, *IAHS Publ.*, 146, 103–114, 1985.
- Valocchi, A. J., Validity of the local equilibrium assumption for modeling sorbing solute transport through homogeneous soils, *Water Resour. Res.*, 21(6), 808–820, 1985.
- Wen, X.-H., and J. J. Gómez-Hernández, Upscaling hydraulic conductivities in heterogeneous media: An overview, *J. Hydrol.*, 183(1–2), ix–xxxii, 1996.
- Wen, X.-H., and J. J. Gómez-Hernández, Numerical modeling of macrodispersion in heterogeneous media: A comparison of multi-Gaussian and non-multi-Gaussian models, *J. Contam. Hydrol.*, 30, 129–156, 1998.
- Zinn, B., and C. Harvey, When is solute spreading described by dispersion, and when is it described by mass transfer? A comparison of upscaled solute transport behavior in multigaussian and well-connected conductivity fields (abstract), *Eos Trans. American Geophysical Union*, 81(48), Fall Meet. Suppl., F410, 2000.

D. L. Freyberg, Department of Civil and Environmental Engineering, Stanford University, Stanford, CA 94305, USA.

A. J. Guswa, Picker Engineering Program, Smith College, Northampton, MA 01063, USA. (aguswa@smith.edu)